The EUMETSAT Network of Satellite Application Facilities

ROM SAF
Radio Occultation Meteorology

ROM SAF CDOP-2

Visiting Scientist Report 30:

ROPP-9.0 beta testing

Feiqin Xie

Danish Meteorological Institute (DMI)
European Centre for Medium-Range Weather Forecasts (ECMWF)
Institut d'Estudis Espacials de Catalunya (IEEC)
Met Office (METO)

Ref: SAF/ROM/DMI/REP/VS/30
Version: 1.0
Date: 4 October 2016

DOCUMENT AUTHOR TABLE

	Author(s)	*Function*	*Date*	*Comment*
Prepared by:	Feiqin Xie	ROM SAF Visiting Scientist	16/9/2016	
Reviewed by (internal):	Ian Culverwell	ROM SAF ROPP Manager	29/9/2016	
Approved by:	Kent B. Lauritsen	ROM SAF Project Manager	3/10/2016	

DOCUMENT CHANGE RECORD

Issue/Revision	*Date*	*By*	*Description*
Draft 1	15/08/2016	F Xie	First draft. Comparison of ROPP and TAMUCC PBLHs.
Draft 2	16/09/2016	F Xie	Second draft. Further comparison against CALIPSO obs.
1.0	4/10/2016	F Xie	Final version. Includes recommendations.

VS Author

The VS study was carried out by Dr. Feiqin Xie, Texas A&M University-Corpus Christi Texas, USA, Email: Feiqin.Xie@tamucc.edu.

VS Duration

The VS study was performed during July - September 2016 at the home institute of the candidate.

ROM SAF

The Radio Occultation Meteorology Satellite Application Facility (ROM SAF) is a decentralised processing center under EUMETSAT which is responsible for operational processing of GRAS radio occultation (RO) data from the MetOp satellites and radio occultation data from other missions. The ROM SAF delivers bending angle, refractivity, temperature, pressure, humidity, and other geophysical variables in near-real time for NWP users, as well as reprocessed data (Climate Data Records) and offline data for users requiring a higher degree of homogeneity of the RO data sets. The reprocessed and offline data are further processed into globally gridded monthly-mean data for use in climate monitoring and climate science applications.

The ROM SAF also maintains the Radio Occultation Processing Package (ROPP) which contains software modules that aids users wishing to process, quality-control and assimilate radio occultation data from any radio occultation mission into NWP and other models.

The ROM SAF Leading Entity is the Danish Meteorological Institute (DMI), with Cooperating Entities: i) European Centre for Medium-Range Weather Forecasts (ECMWF) in Reading, United Kingdom, ii) Institut D'Estudis Espacials de Catalunya (IEEC) in Barcelona, Spain, and iii) Met Office in Exeter, United Kingdom. To get access to our products or to read more about the ROM SAF please go to: http://www.romsaf.org

Intellectual Property Rights

List of Contents

Executive Summary

The planetary boundary layer (PBL) is one of the key components of the weather and climate system that controls the exchanges of energy, mass and momentum between the earth's surface and the free troposphere. The PBL height is a crucial parameter in the PBL process. The PBLH diagnostics derived from GPS Radio Occultation (RO) measurements could provide a critical dataset to help understand the complicated PBL processes and improve the PBL parameterization in weather and climate models.

In this project, the beta version of the ninth major release of the Radio Occultation Processing Package (ROPP-9.0) was downloaded, installed and evaluated. The major focus is to assess the robustness and scientific integrity of the ROPP planetary boundary layer height (PBLH) diagnostics. Three-month GPS RO soundings (over 180,000 occultation events) from five RO missions, along with the collocated model profiles from the UK MetOffice during March-April-May of 2013 were processed with the ROPP PBLH diagnostic tool. Overall, the ROPP application tool is robust and easy to use, and the documentation is clear and very well-structured.

The ROPP PBLH diagnostics include three PBLHs based on RO parameters (refractivity, bending angle and dry temperature) along with three other PBLHs based on model parameters (specific humidity, relative humidity and temperature). The median of the six PBLH seasonal climatology were derived. Furthermore, the ROPP PBLH diagnostics are directly compared with the independent PBLH product retrieved at the Texas A&M University – Corpus Christi, which uses similar gradient method for PBLH detection. Both PBLH global products are highly consistent with each other. However, significant positive biases are seen in ROPP PBLH over the polar regions. In addition, the sharpness parameter for each physical parameters is also presented, which measures the relative magnitude of the gradient and could be a good indicator of the robustness of the PBLH diagnostic. Finally, the ROPP PBLH diagnostics are compared to the CALIPSO lidar PBLH measurements. The best agreement are seen over tropics, subtropics and mid-latitude (from ~50°S to ~60°N). Again, ROPP PBLHs show largest biases over polar regions. The positive biases in ROPP PBLHs over the Antarctic and Greenland are likely due to the special treatment of ROPP PBLH detection algorithm in the presence of shallow surface inversion and require some further investigation. In addition, the ROPP dry temperature based PBLH also shows large positive bias over the tropics in comparison to CALIPSO PBLH, which requires further investigation.

1. Introduction

1.1 Purpose of Document

This document contains the results from the ROM SAF Visiting Scientist activity on testing the ninth version of the Radio Occultation Processing Package (ROPP) with the focus on assessing the robustness and scientific integrity of the ROPP planetary boundary layer height (PBLH) diagnostics.

1.2 The Planetary Boundary Layer Height Observation from GPS Radio Occultation

The planetary boundary layer (PBL) is one of the key components of the weather and climate system that controls the exchanges of energy, mass and momentum between the earth's surface and the free troposphere (Garratt 1992). The top of the PBL is generally a thin transition layer (a few hundred meters) marked by a temperature inversion or negative moisture gradient. The PBL height (PBLH) is a crucial parameter in the PBL process, which measures the vertical scale of turbulent eddies. The shallow PBL (1~3 km) with the frequent low cloud presence is very challenging to measure from the space, and simulated in weather/climate models. The conventional PBL measurements are restricted to sparse towers, radiosonde soundings and some field campaigns. The limited spatial and temporal coverage of PBL observations hinders the understanding of complex PBL processes and leads to poor representation and prediction skills of the PBL evolution and the associated low cloud formation in the weather and climate models (e.g., Duynkerke and Teixeira, 2001; Bretherton et al., 2004; Bony and Dufresne, 2005; Stephens, 2005; Soden and Held, 2006; Wyant et al., 2006; Clement et al., 2009). Continuously monitoring the global PBLH will provide a critical dataset to evaluate various PBL parameterization schemes through the diagnostic analysis and combat the related model uncertainty issues.

The satellite-based GPS radio occultation (RO) technique offers high vertical resolution, global measurement of atmospheric vertical structure in all-weather condition, which has demonstrated its capability to provide the global PBLH observations (e.g., Sokolovskiy et al. 2006, Ao et al., 2012, Xie et al., 2012, etc.). In this report, we focus on the analysis of GPS RO soundings collected from multiple satellite RO missions along with the collocated model profiles from the UK MetOffice during March-April-May (MAM) of 2013. The PBLH diagnostic product generated by the beta version of ROPP-9.0 package are evaluated and compared to an independent PBLH product generated at Texas A&M University – Corpus Christi (TAMU-CC) as well as the CALIPSO satellite lidar measurements.

The document is organized as follows: Section 2 contains the general experience of downloading, installation and usage of the ROPP package. Section 3 describes the derivation and evaluation of the PBLH diagnostic product from ROPP. The seasonal median PBLH climatology during MAM of 2013 were generated. The difference among PBLH diagnostics were presented. The ROPP PBLH products are also directly compared to the PBLH product developed at TAMU-CC. Moreover, the ROPP PBLH diagnostics are also compared to the CALIPSO lidar PBLH measurement during the same period. The

major conclusions and suggestions are summarized in the Section 4. Finally, the references and the list of acronyms are presented in Section 5 and 6 at the end of this document.

2. General Assessment of the Beta Release of ROPP-9.0

2.1 Download of the Beta Release of ROPP-9.0

The beta release of ROPP-9.0 software and the associated documentation were successfully downloaded from ROM SAF website without encountering problems. Both the single file tarball and the individual files of the software package were separately downloaded and unpacked without any issue.

2.2 Installation and General Utility of the Software Package

The beta release of ROPP-9.0 were successfully installed on the computer server at Texas A&M University – Corpus Christi (TAMU-CC) with the following configuration:

- CPU: Intel(R) Xeon(R) CPU E5-2440 0 @ 2.40GHz
- OS: Scientific Linux release 6.8 (Carbon)
- Compiler: gfortran

The step-by-step installation guideline described in ROPP Release Notes (Version 9.0) is well structured and is clear and easy to follow.

The only suggestion is to make it clear that the default shell environment is in *bash* while using "*export*" command. Alternatively, the "*setenv*" command for C-shell (*csh*) or T-shell (*tcsh*) environment could be added, such as follows:

- export ROPP_ROOT=/usr/local # bash
- setenv ROPP_ROOT /usr/local # csh/tcsh

The main package used for this report is the ROPP Application package (ROPP_APPS), which provides various ROPP APPS library. More specifically, the ROPP application tool are used to derive the diagnostics of the planetary boundary layer height. The test folder and the readme files are very helpful for the user to understand the usage of the shell script and Fortran programs as well as the input and output data format. The output data in NetCDF format is especially helpful and convenient for the users to carry out further data processing and analysis.

3. Assessment of the PBLH Diagnostics

3.1 Generate PBLH Diagnostics with ROPP

Three months of GPS radio occultation (RO) dataset during March-April-May (MAM) of 2013 (~62,000 soundings per month) were provided for evaluating the PBLH diagnostic products. The RO data is obtained from internal "Obs Processing System" (OPS) of the UK MetOffice. The dataset contains the daily GPS RO bending angle, refractivity profiles from several RO missions, as well as the collocated temperature, specific humidity profiles from the UK MetOffice model analysis. The GPS RO soundings are collected from five RO satellite missions, including the COSMIC (~53.6%, missing COSMIC-3), MetOp-A (~24.5%), Terra-SAR-X (~10.8%), C/NOFS (~6.5%) and GRACE-A (~4.6%), with the percentage based on RO data in April 2013. The RO data from March and May share similar fractional distribution among RO missions. Each file in the dataset includes the daily RO soundings in NetCDF format. The RO sounding parameters, including refractivity, bending angle and geopotential/geometric heights are reported at 247 vertical levels with ~200m interval from surface up to ~60 km. In addition, the parameters of collocated model analysis, such as temperature, specific humidity and relative humidity are reported at 70 vertical grids from surface up to ~80 km, with about 200 m vertical interval below 2 km and increased sampling interval at higher altitude.

The ROPP PBLH APPS tool generates six PBLH diagnostics based on GPS RO refractivity ($PBLH_N$), bending angle ($PBLH_\alpha$), and dry temperature ($PBLH_{Tdry}$), as well as the collocated model background specific humidity ($PBLH_q$), relative humidity ($PBLH_{rh}$), and temperature ($PBLH_T$) based on the gradient method. Detailed description of the PBLH algorithm can be found in ROM SAF (2016b,c). Each PBLH diagnostic reports the height (geopotential and/or geometric heights) of the minimum gradients ($PBLH_{N,\alpha,q,rh}$) or maximum gradients ($PBLH_{Tdry,\ T}$) for the specific parameter in the profile. The value of the parameter at the PBLH is also reported. In addition, the height for a second minimum or maximum gradient of each profile along with the parameters at that height are also reported. In this study, only the PBLH diagnostics are evaluated. Note that the daily ROPP input files used for the study follow the input data structure guideline described in ROM SAF (2016a). The following command can then be used to generate the PBLH diagnostics given the input file name:

- *ropp_apps_pblh_tool* "input RO file name" *–o* "output PBLH file name" *–d*

The output file includes six PBLH diagnostics derived from three RO parameters and three collocated model parameters in NetCDF format. With the "*-d*" option, the PBLH diagnostics will be appended to the original NetCDF file that contains RO and model profiles.

Note that the RO dry temperature profiles are absent in the original dataset. The ROPP application package will derive the dry temperature profiles from the refractivity (e.g., ropp_apps/common/ropp_apps_calc_tdry.f90) and further derived the $PBLH_{Tdry}$ with the gradient method. Similarly, the relative humidity is not a standard ROPP background field and is derived from the specific humidity and temperature before the calculation of $PBLH_{rh}$.

No major issues were found during the processing of the large dataset. In a few cases, however, some missing parameters in the ROPP input data file could lead to failed PBLH diagnostics generation. It might be worth an effort to develop more robust algorithm that will allow to skip the processing of the missing parameter(s) in the input file.

3.2 Evaluate the Scientific Integrity of ROPP PBLH Diagnostics

3.2.1 Global Distribution of GPS RO Soundings

Note that not all the RO soundings penetrate deep into the PBL. To avoid the bias in PBLH detection due to the limited vertical range of RO sounding, those profiles that did not penetrate deep into the PBL need to be excluded. The global map of one-month RO soundings distribution (~62,000) at 5°latitude × 5°longitude grid in April 2013 is shown in Figure 1a. The gridded RO sounding number varying from a minimum of few soundings in the tropics and polar regions to a maximum of ~50 in mid-latitude. In the ROPP algorithm, only the RO soundings reach below 300 m above the local surface will be used for PBLH derivation (ROM SAF, 2016b,c). The penetration criteria significantly reduces the valid RO soundings used for PBLH derivation, especially near tropics where fewer than 10 RO profiles in many grids (Fig. 1b).

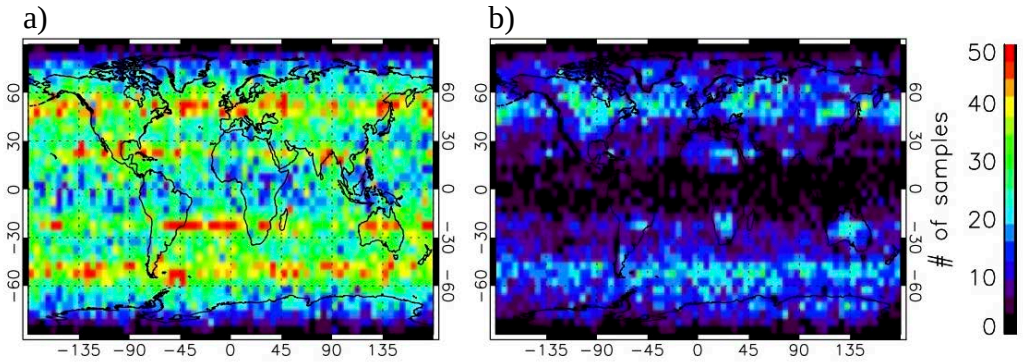

Figure 1. GPS RO profile distribution in April 2013 with 5° latitude × 5° longitude grid. (a) number of GPS RO profiles (including COSMIC, MetOp-A, GRACE-A, C/NOF and TerraSAR); (b) number of RO profiles used for PBLH derivation that penetrate below 300 m above the surface.

To increase the gridded RO sounding numbers especially over the tropics, two more months (March and May) of RO soundings were added. The overall RO grid sample significantly increases with a maximum reaching over 100 in the subtropics and mid-latitude (Fig. 2a). The valid RO soundings that reach below 300 m also increases (Fig. 2b). Note that several RO satellites, such as GRACE-A and C/NOF are equipped with the close-loop tracking receiver. The increasing tracking errors in the moist lower troposphere lead to degraded data quality and fewer soundings penetrating within the lowest few kilometers of the atmosphere (e.g., Beyerle et al., 2006). MetOp-A also have some data quality issues in the moist lower troposphere due to the combination of receiver issue and geometric optic processing (e.g., Lauritsen et al., 2011). On the other hand, both COSMIC and TerraSAR-X are equipped with the open-loop tracking receivers (Sokolovskiy 2001; Ao et al., 2009) that allow high-quality RO to probe deep into the moist lower troposphere

and are therefore best fit for PBLH study. The RO sounding maps for only COSMIC and TerraSAR-X are also shown, which shows almost 50% deduction of the total RO sounding numbers (Fig. 2c). However, the numbers of valid RO sounding that penetrating below 300 m (Fig. 2d) is rather consistent with what is shown in Fig. 2b, especially over the tropics. This indicates a majority of RO soundings over tropics from MetOp-A, C/NOFs and GRACE-A were discarded for ROPP PBLH processing due to the limited penetration.

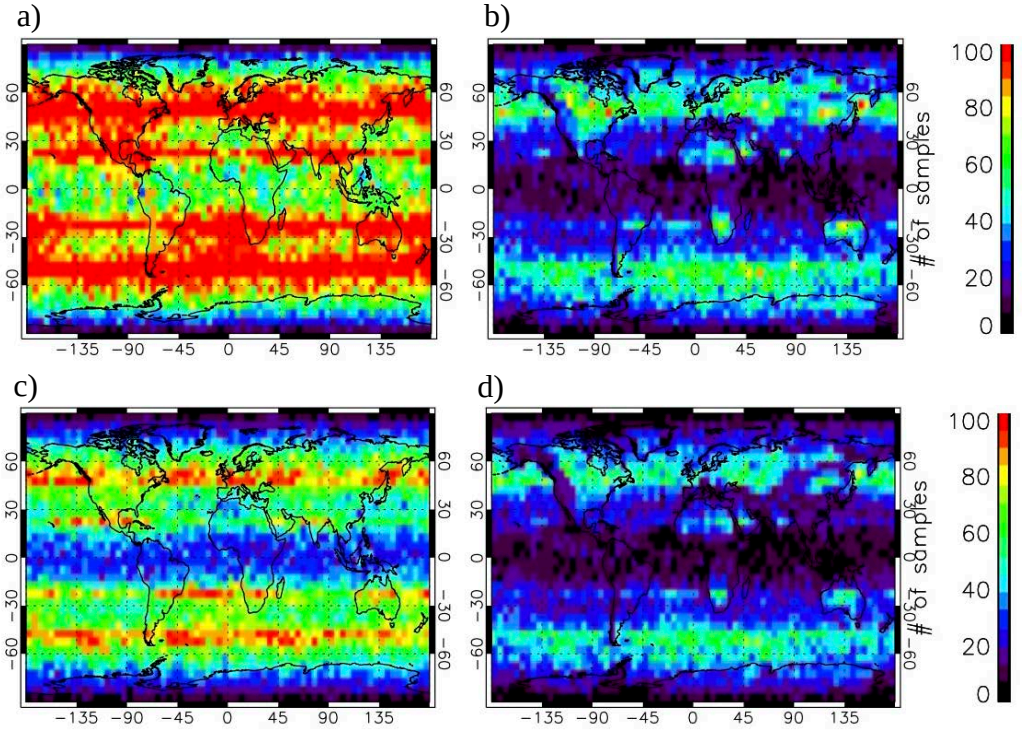

Figure 2. GPS RO profile distribution during March-April-May of 2013 with 5° latitude × 5° longitude grid. (a) total number of RO profiles and (b) number of RO profiles penetrating below 300 m from all five RO missions; (c) total number of RO soundings and (d) number of RO profiles penetrating below 300 m from COSMIC and TerraSAR-X only.

The percentage of deep penetrating RO profiles that reach the lowest 300 m above the local surface is mapped in Fig. 3. A very low percentage (only 10-20%) deep penetrating soundings are seen over the tropics. Over 50% and even higher are seen over mid-latitude and polar regions, respectively. Note again, most of the deep penetrating RO profiles are from COSMIC and TerraSAR-X.

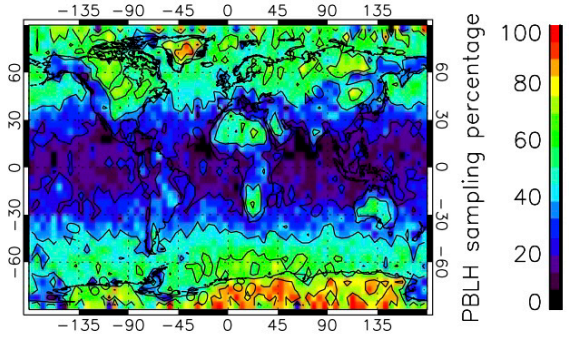

Figure 3. The percentage of the RO profiles from all five RO missions used for PBLH derivation that penetrate below 300 m above surface, during March-April-May of 2013.

3.2.2 ROPP PBLH Diagnostics Analysis

3.2.2.1 Seasonal Climatology of the ROPP PBLH Diagnostics

ROPP PBLH diagnostics were generated based on the three-month RO sounding data during MAM of 2013. Three PBLH diagnostics are based on RO bending angle, refractivity, and dry temperature, and the other three are based on model background specific humidity, relative humidity, and temperature from UK MetOffice. The PBLH diagnostics are then binned into 5° latitude × 5° longitude grid. The seasonal median PBLH climatology based on the six physical parameters (e.g., refractivity $PBLH_N$, bending angle $PBLH_\alpha$, dry temperature $PBLH_{Tdry}$, specific humidity $PBLH_q$, relative humidity $PBLH_{rh}$, and temperature $PBLH_T$) during MAM of 2013 are shown in Fig. 4. The PBLH diagnostics derived from RO parameters (left column) and the model parameters (right column) reveal similar global pattern with highest PBLH over subtropical land (especially over the Sahara desert), and relatively shallow PBLH over high latitudes. The distinct dipole PBLH structure are shown in all six PBLH diagnostics, which features a transition from a shallow PBLH (~1 km) near the stratocumulus regime over the subtropical eastern ocean near the western coast of the continent, to a much deeper PBLH (~2 km) off shore into the trade cumulus regime (Guo et al., 2011, Xie et al., 2012). It is worth noting that large difference are shown among six PBLH diagnostics especially over the tropics and the polar regions. For example, the $PBLH_\alpha$ and $PBLH_{Tdry}$ show deeper PBLH over tropics as comparing to all other PBLHs. The three model PBLH all show very shallow PBLH near the topical ITCZ (Intertropical Convergence Zone) region.

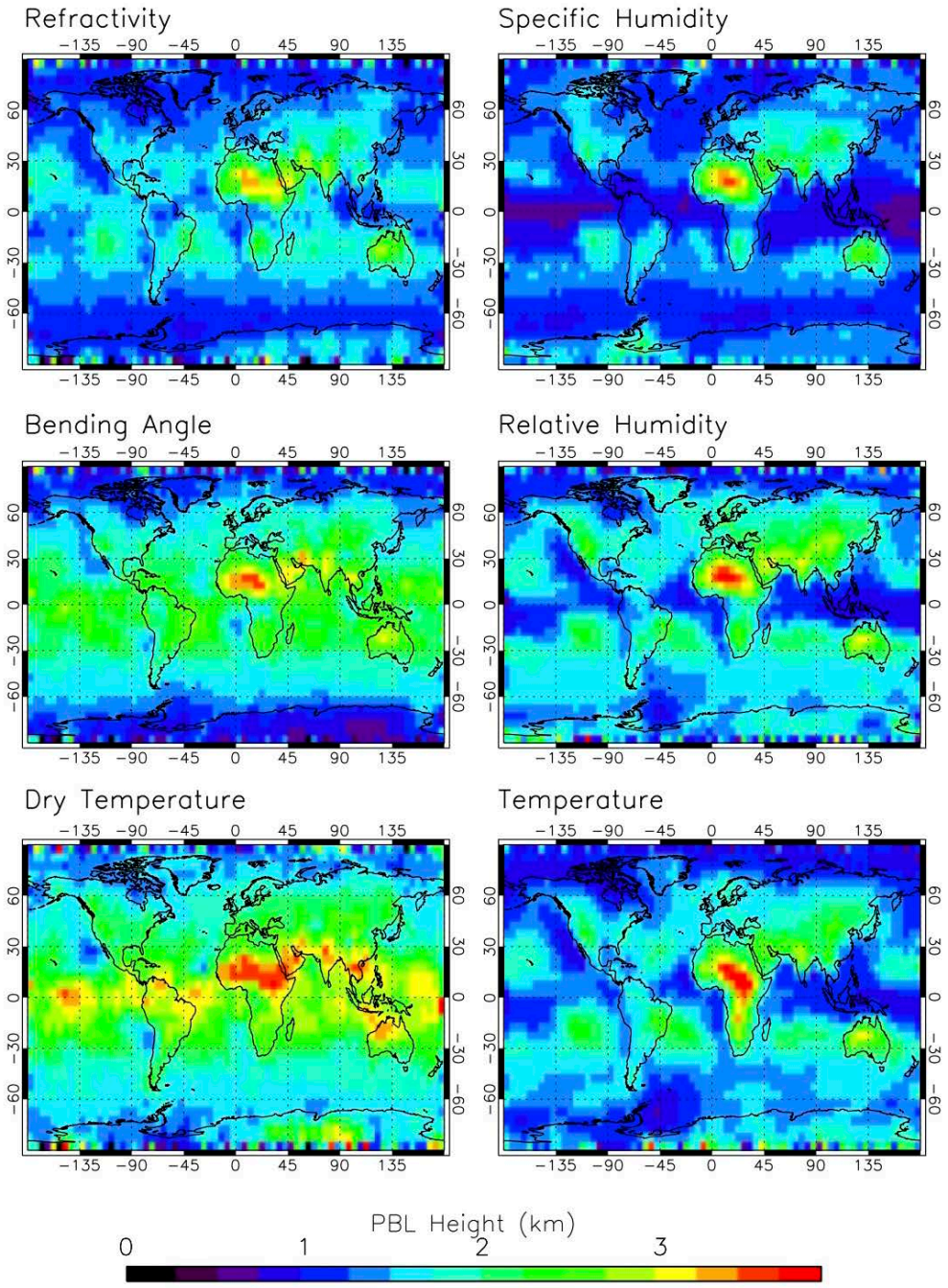

Figure 4. Median of seasonal ROPP PBLH climatology based on GPS RO refractivity, bending angle and dry temperature (left), as well as the collocated model specific humidity, relative humidity and temperature from the UK MetOffice analysis during March-April-May of 2013.

Furthermore, the variation of the PBLH in terms of the median absolute deviation (MAD) for the six different PBLH climatology can be seen in Fig. 5. The lowest MAD (<300 m) is seen over the subtropical eastern ocean near the western coast of the continent. Note however, the model PBLHs show smaller variation over subtropical eastern ocean than RO. On the other hand, the largest variation of RO PBLHs are mostly found over land and the tropical oceans as seen in $PBLH_{\alpha}$ and $PBLH_{Tdry}$. It is also interesting to note the large MAD found in refractivity, dry temperature and relative humidity based PBLH over Antarctic, which will be discussed further in later section.

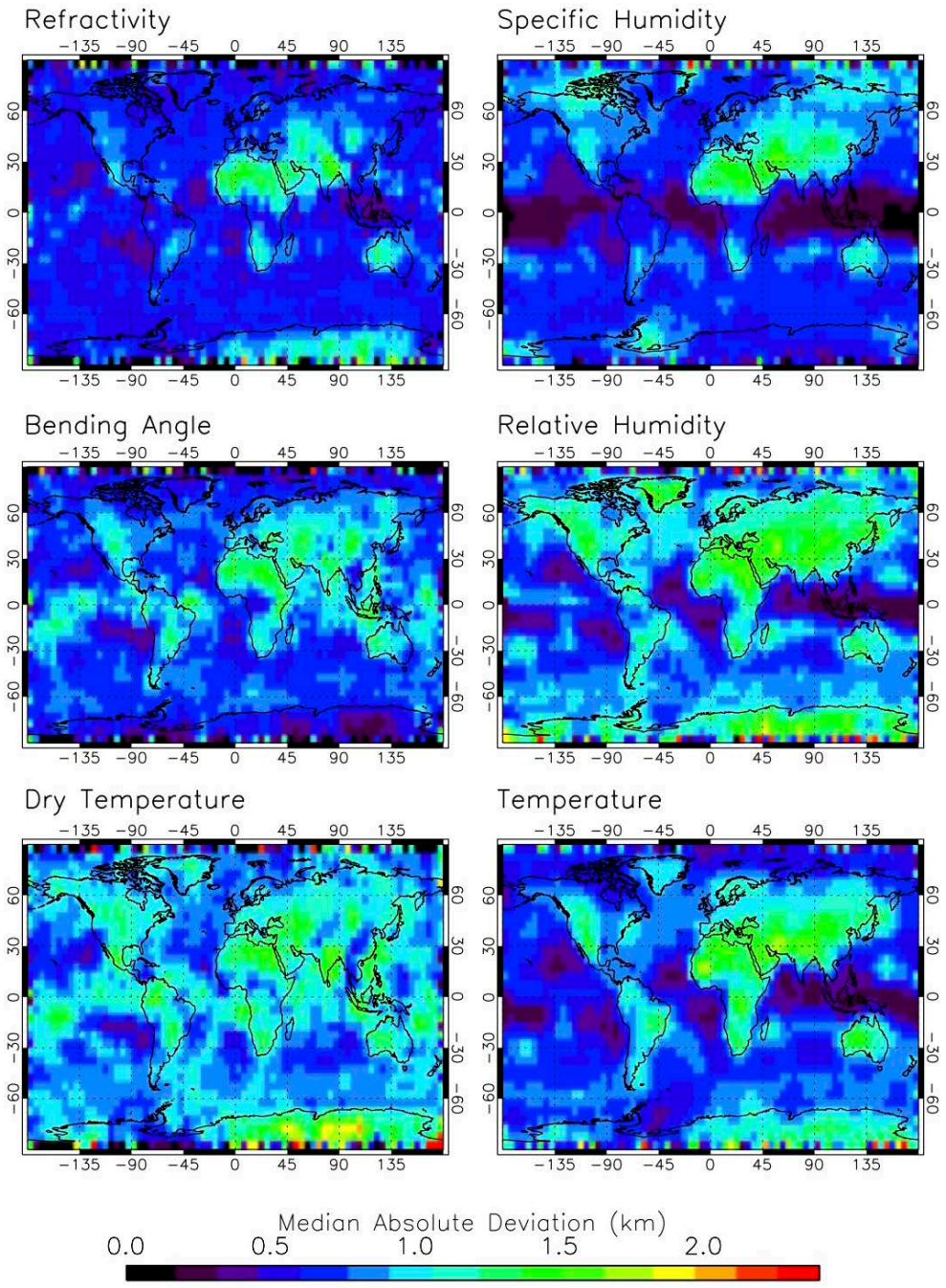

Figure 5. Median absolute deviation (MAD) of ROPP PBLH seasonal climatology based on GPS RO refractivity, bending angle and dry temperature (left), as well as the collocated model specific humidity, relative humidity and temperature from the UK MetOffice analysis during March-April-May of 2013.

3.2.2.2 Intercomparison of ROPP PBLH Diagnostics Based on Different Parameters

As discussed in Xie (2014), PBLH diagnostics derived from different physical parameters based on the gradient method could be quite different due to the different sensitivity of the specific parameter's gradient to temperature and/or specific humidity gradients. The difference between individual PBLH climatology and the seasonal median $PBLH_N$ climatology are shown in Fig. 6. General consistency are seen among all PBLH diagnostics, with the major difference seen over the tropics and polar regions. The $PBLH_q$ shows largest negative bias comparing to $PBLH_N$. The $PBLH_{Tdry}$, on the other hand, shows largest positive bias compared to $PBLH_N$ but mainly over the tropics. The relative weak temperature and humidity gradient along with a wide range of variations over the topical ocean could contribute to the large difference among PBLH diagnostics. On the other hand, large negative bias is seen in $PBLH_\alpha$ over the Antarctic, which needs further study.

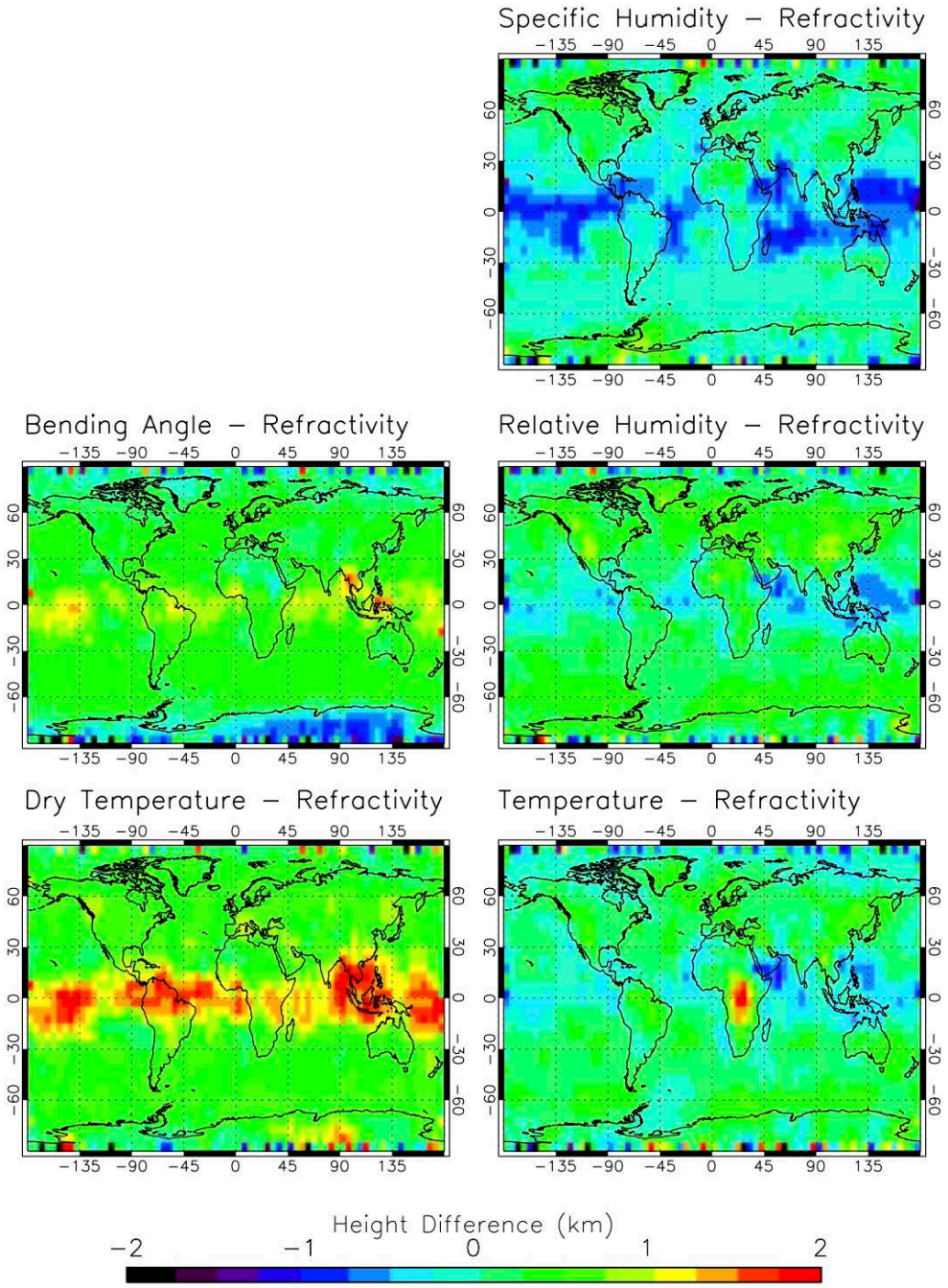

Figure 6. Difference between individual ROPP PBLH diagnostic and the seasonal median climatology of $PBLH_N$ during March-April-May of 2013.

3.2.3 PBLH Diagnostics at Texas A&M University – Corpus Christi

Note that Xie and his group at the Texas A&M University – Corpus Christi (TAMU-CC) developed and maintained their own algorithm to derive the PBLH diagnostics from GPS RO measurements. The TAMU-CC PBLH algorithm uses gradient method detailed in Xie et al. (2012) and Xie (2014).

Similar to the ROPP PBLH algorithm, the input profile is required to reach at or below a minimum penetration height (h_{penet}) threshold above the local surface. In addition, the minimum (h_{min}) and maximum (h_{max}) cut-off heights are introduced to specify the valid vertical range in searching for the height of minimum (or maximum) gradient as the PBLH. To be consistent with the ROPP PBLH diagnostics analysis, we set both h_{penet} and h_{min} to be 300 m and h_{max} = 5 km.

Note that the two parameters (h_{penet} and h_{min}) do not need to be the same. As seen in Fig. 3, only about 10% GPS RO profiles penetrating below 300 m over the moist tropics. Increasing h_{penet} would allow more RO soundings to be used for PBLH diagnostic. But a higher threshold of h_{penet} could potentially introduce a positive bias to the PBLH diagnostics. The h_{min}, on the other hand, is used to discard the lowest portion (e.g., 300 m) of the profile near surface, where sharp gradient related to the surface inversion are often observed over oceans.

The RO profile (e.g., refractivity, dry temperature, etc.) is then interpolated on a 10-m vertical grid before the gradient calculation to find the PBLH diagnostics over the range from h_{min} to h_{max}.

To quantify the robustness of the PBLH diagnostics derived from the gradient method, the sharpness parameter (Ao et al., 2012) for each profile is also computed as follows:

$$\tilde{X}' \equiv -\frac{X'_{min}}{X'_{RMS}} \qquad (1)$$

where, X and X' is the physical parameter (e.g., refractivity, temperature etc.) and its gradient, X'_{RMS} is the root-mean square (RMS) value of X' average over the altitude range considered, in this case, from 300 m to 5 km.

Recommendation:

It could be useful to include the minimum penetration height (h_{penet}) as a separated input parameter, instead of a hard-coded parameter. A slight increase the threshold could help increase the useful RO soundings for regional studies. For example, a threshold of 500 m was used in Xie et al. (2012) over subtropical southeast Pacific Ocean.

In addition, two more input parameters: the minimum and maximum cut-off height (e.g., h_{min} = 300 m, h_{max} = 5 km) could be introduced, which specifies the valid vertical range of RO profiles to be used for PBLH derivation. The input parameter h_{min} could be different from h_{penet}. Also it could be very useful to change it to be even less than 300m when trying to identify the surface inversion that are often seen over polar regions and the nocturnal PBL over land. However, the RO sounding quality near the surface is still lack of understanding and need more studies.

3.2.3.1 Seasonal Climatology of the TAMU-CC PBLH Diagnostics

Similar to the ROPP processing, the PBLH diagnostics for the six parameters are derived and binned into 5° grid at TAMU-CC. As discussed in Section 3.1, the RO dry temperature profiles are absent in the original RO dataset. Here we compute the dry pressure (P_{dry}) by removing the water vapor pressure from the total pressure in the model profile. Then the dry temperature (T_{dry}) profile can be derived from the RO refractivity through $T_{\mathrm{dry}} = 77.6\, P_{\mathrm{dry}}/N$.

The seasonal median PBLH climatology during MAM of 2013 is shown in Fig. 7, which show very similar patterns over tropics and mid-latitude as revealed in ROPP PBLH climatology (Fig. 4). However, much shallower PBLHs are seen in both poles in all three RO PBLHs along with the model PBLH_T as compared to ROPP PBLH diagnostics.

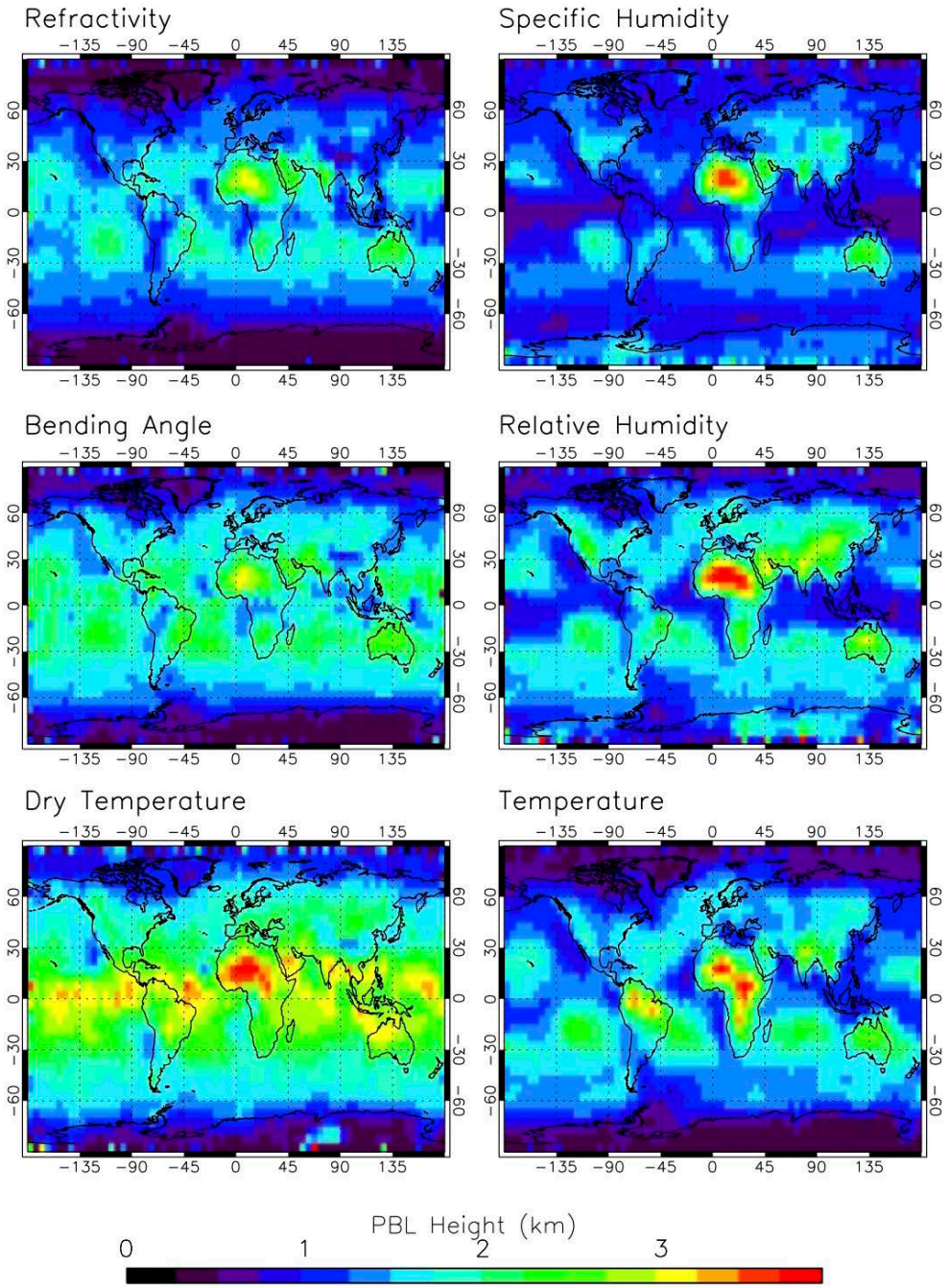

Figure 7. Median of seasonal TAMU-CC PBLH climatology based on GPS RO refractivity, bending angle and dry temperature soundings (left), as well as the collocated model specific humidity, relative humidity and temperature from the UK MetOffice analysis during March-April-May of 2013.

Similar to Figure 5, the median absolute deviation (MAD) of the six different PBLH climatology is shown in Fig. 8. Again very similar patterns are seen in TAMU-CC PBLH. But the amplitude of MAD is slightly larger in TAMU-CC product over the tropics and the mid-latitude. Whereas, much smaller MAD is seen over polar regions for all three RO PBLHs and the $PBLH_T$.

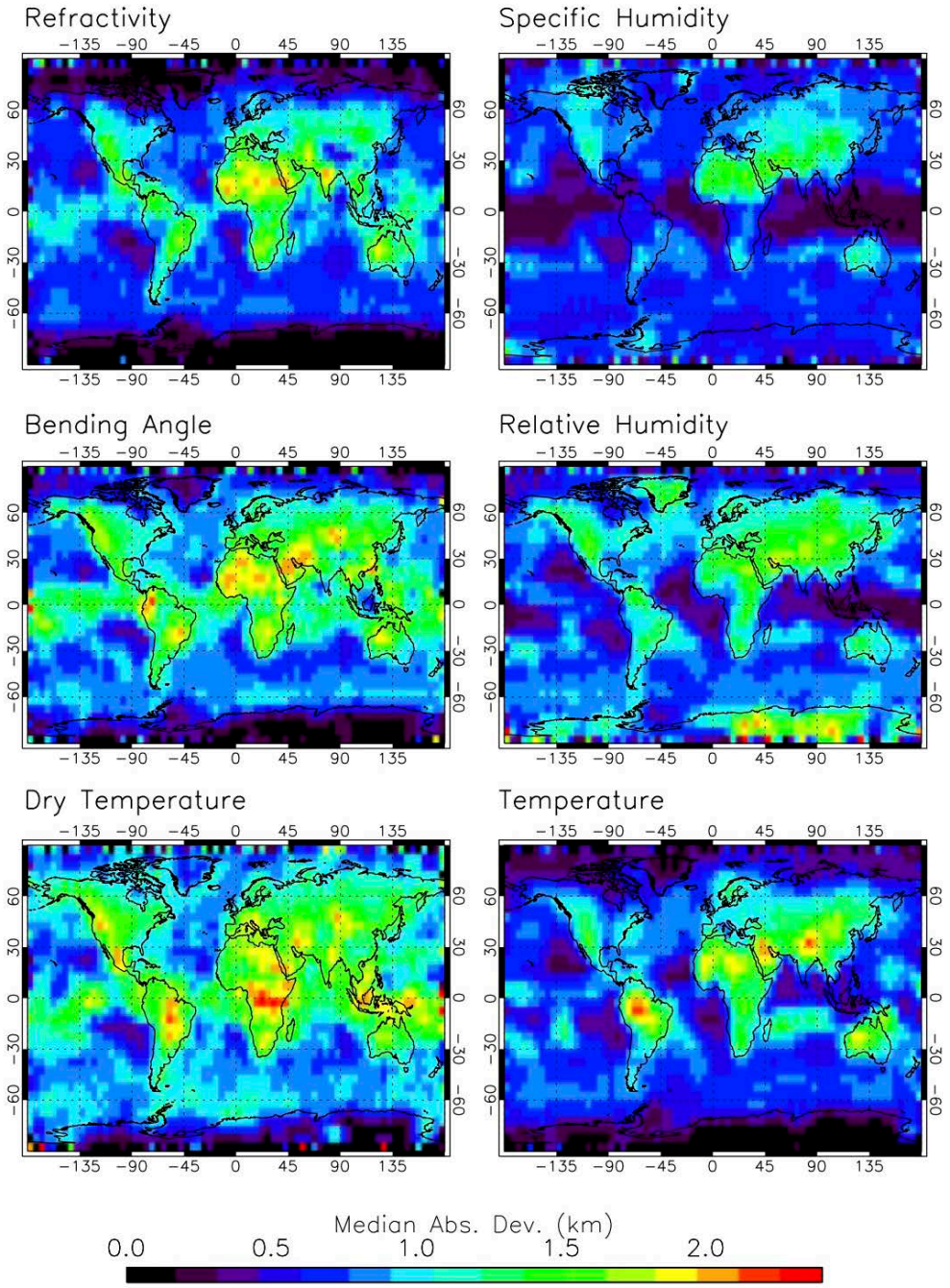

Figure 8. Median absolute deviation (MAD) of TAMU-CC PBLH seasonal climatology based on GPS RO refractivity, bending angle and dry temperature (left), as well as the collocated model specific humidity, relative humidity and temperature from the UK MetOffice analysis during the March-April-May of 2013.

3.2.3.2 Intercomparison of TAMU-CC PBLH Diagnostics Based on Different Parameters

The difference between individual TAMU-CC PBLH climatology and the seasonal median $PBLH_N$ climatology are shown in Fig. 9. Again, the overall pattern of the PBLH difference is very close to the difference in ROPP PBLH diagnostics (Fig. 6). All three model PBLH

diagnostics, especially $PBLH_q$ and $PBLH_{rh}$ shows low bias over tropical oceans. Note, however, some major differences are mainly see over the Antarctic except the $PBLH_{Tdry}$ and $PBLH_T$.

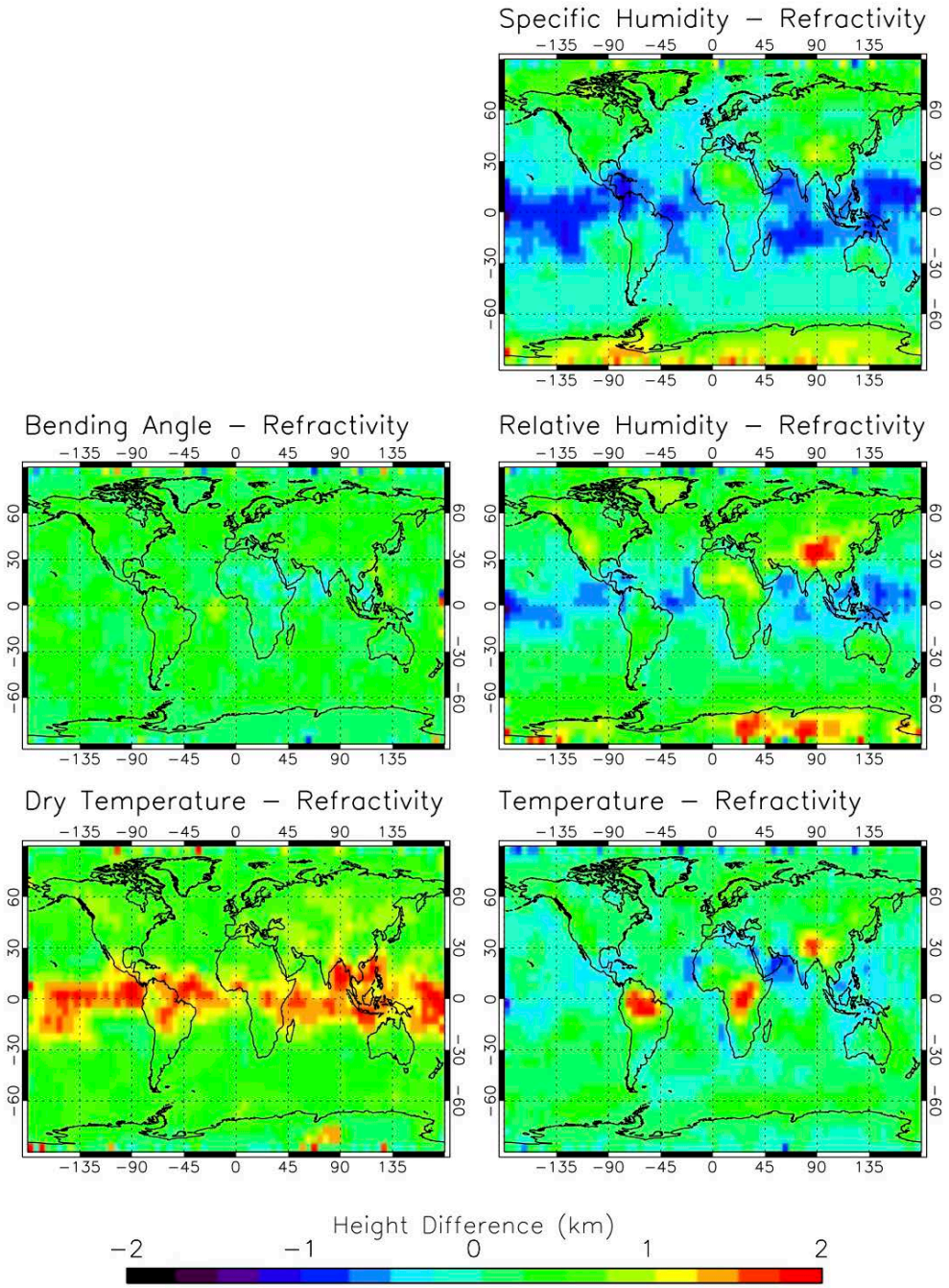

Figure 9. Difference between individual TAMU-CC PBLH diagnostic and the seasonal median climatology of refractivity-based PBLH during March-April-May of 2013.

To evaluate the robustness of the PBLH diagnostics, the sharpness parameter (Ao et al., 2012) for each physical parameter were derived. The seasonal median of the sharpness parameter is shown in Fig. 10. The strongest sharpness parameter were shown over the subtropical eastern ocean for all six parameters, which explains the minimum difference among various PBLH diagnostics.

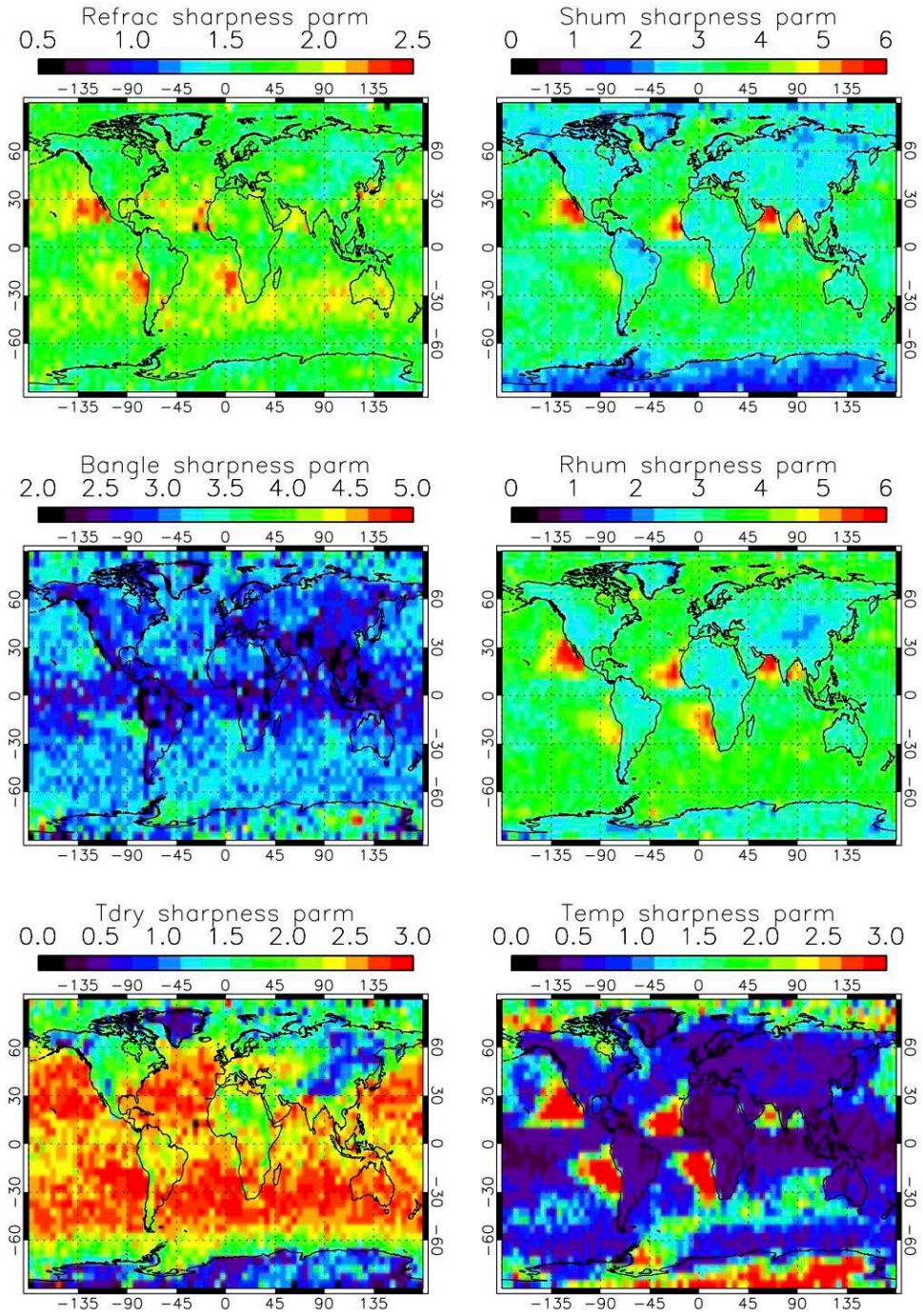

Figure 10. Seasonal median of sharpness parameter for TAMU-CC PBLH diagnostics.

Recommendation:

Add the sharpness parameter for each PBLH diagnostic, which is currently missing in ROPP PBLH product.

3.2.4 Comparison Between ROPP and TAMU-CC PBLH Diagnostics

The seasonal climatology of ROPP PBLH diagnostics are compared to the TAMU-CC PBLH product with the difference shown in Fig. 11. The two PBLHs are overall very consistent with each other, especially seen in $PBLH_q$ and $PBLH_{rh}$. However, the TAMU-CC PBLH shows lower PBLH as compared to ROPP product over the polar region and some over tropics on the other four PBLH diagnostics.

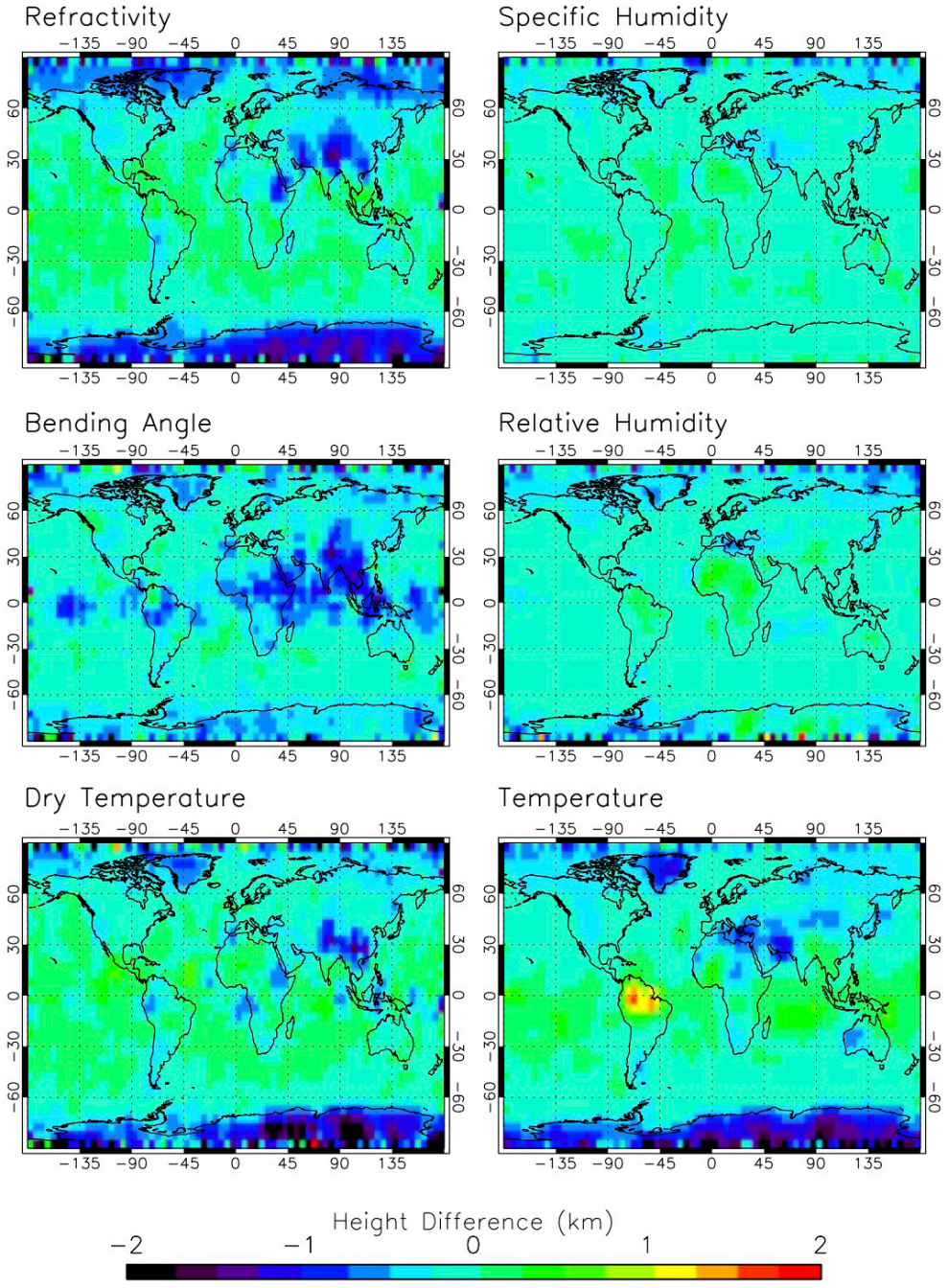

Figure 11. Difference of seasonal median TAMU-CC PBLH climatology from ROPP during the MAM of 2013.

We further investigate the RO refractivity and model temperature gradient profiles over the Antarctic (85°S-90°S). Six typical cases are shown in Fig. 12. The $PBLH_N$ and $PBLH_T$ derived from both ROPP and TAMU-CC are shown, respectively. An obvious and dominant surface inversion is present in all six cases with the largest gradient below 300 m and very close or at the surface. As both algorithm search for the minimum (*N*) and maximum (*T*) gradient above 300 m, the TAMU-CC consistently identify the height of the minimum gradient ($PBLH_N$) and maximum gradient ($PBLH_T$) close to the threshold height of 300m. On the other hand, the ROPP algorithm seems to skip the lowest maximum/minimum gradient and identify a much higher PBLH. The way that ROPP PBLH diagnostics in the presence of surface inversion seems to be deviating from the typical "local maximum/minimum" gradient method, which is also discussed in ROM-SAF Report 24 (ROM SAF, 2016c). This could complicate the interpretation of the PBLH product. Clarification of the treatment of PBLH detection in the presence of one dominating surface inversion is needed.

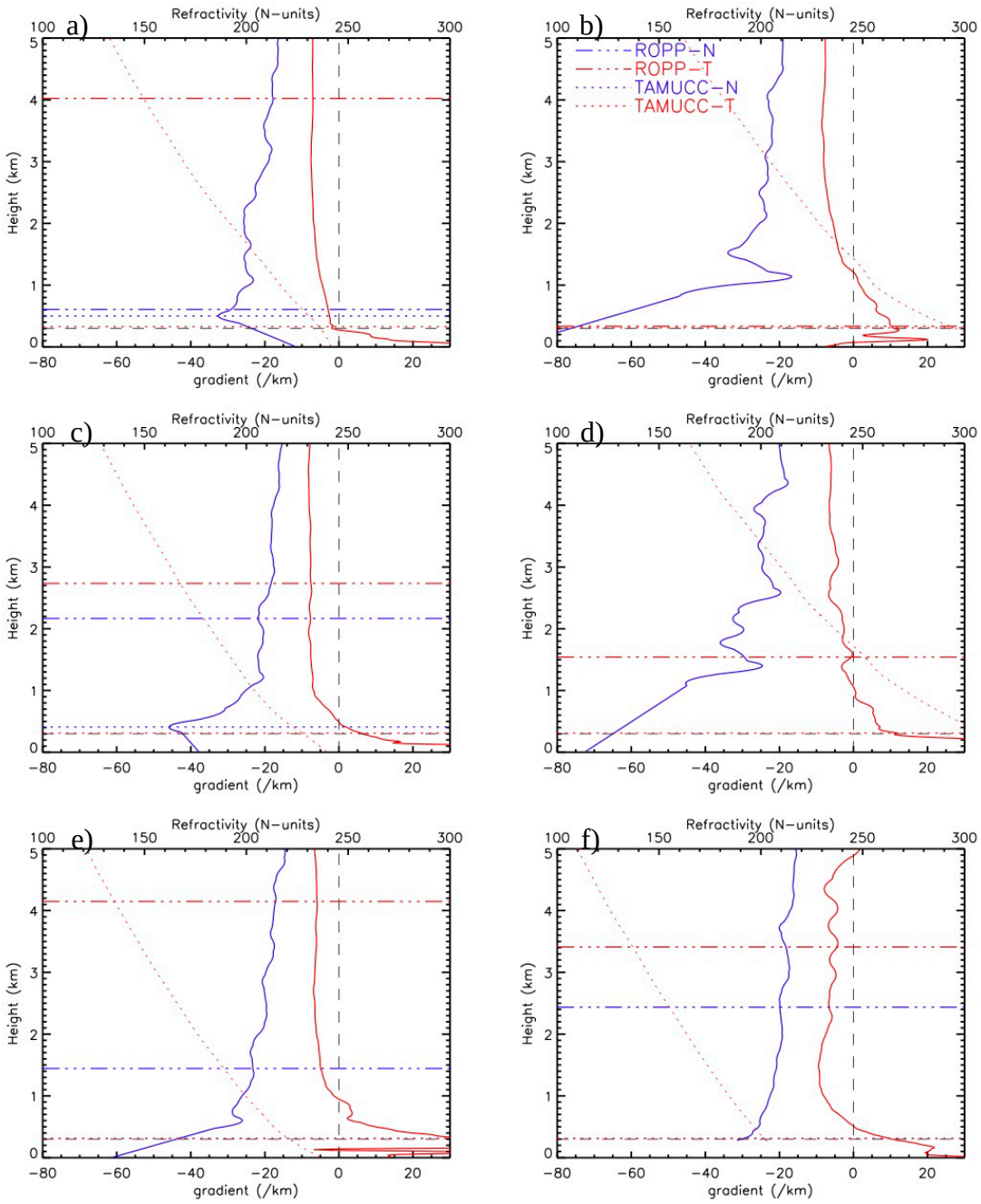

Figure 12. Six typical GPS RO refractivity profile (red-dotted) and the vertical gradients of RO refractivity and model temperature over the Antarctic (85°S-90°S). The $PBLH_N$ and $PBLH_T$ for both ROPP (dash-dotted) and TAMU-CC (dotted) are marked by the horizontal lines.

3.2.5 Comparison Between ROPP PBLH Diagnostics and CALIPSO Observations

It is worthy noting that low clouds or aerosol layers are normally trapped inside the PBL. Such height of low cloud or aerosol layer could be a very good indicator of the PBLH

(Jordan et al., 2010; Ho et al., 2015). The Cloud-Aerosol Lidar and Infrared Pathfinder Satellite Observations (CALIPSO) lidar measures backscattering of linearly polarized laser light at 1064 nm and 532 nm wavelengths from near nadir-viewing geometry and retrieves cloud and aerosol profiles since 2006 (Winker et al. 2007). With a superb vertical resolution, the CALIPSO lidar is considered as one of the most accurate cloud remote sensing instruments in terms of unambiguously distinguishing between clouds and surfaces. Global observation of the low cloud-top-height (CTH) and/or low-level aerosol-layer-height offer an independent way of sensing the global PBLH when low clouds and/or aerosol layers are present inside the PBL.

The CALIPSO Level-1B backscattering data from MAM of 2013 are analyzed. The vertical resolution of the lowest 8.2 km is averaged to 60 m. The horizontal bins are averaged to 1km resolution and a 15-km running mean is applied. The clouds are reported as cloud layers (characterized by pairs of top and base heights) with 1 km horizontal resolution and 60 m vertical resolution (Wang et al., 2008, Adhikari et al., 2010).

The gridded median of the seasonal PBLH climatology derived from CALIPSO during MAM of 2013 is shown in Fig. 13a. The variation, i.e., the median-absolute-deviation, of the PBLH within each 5° grid is shown in Fig. 13b. Very similar PBLH structure, especially over the ocean are shown in comparison to the ROPP PBLH climatology. Over mid to high latitude, however, CALIPSO shows generally higher PBL except over the Antarctic and the Greenland.

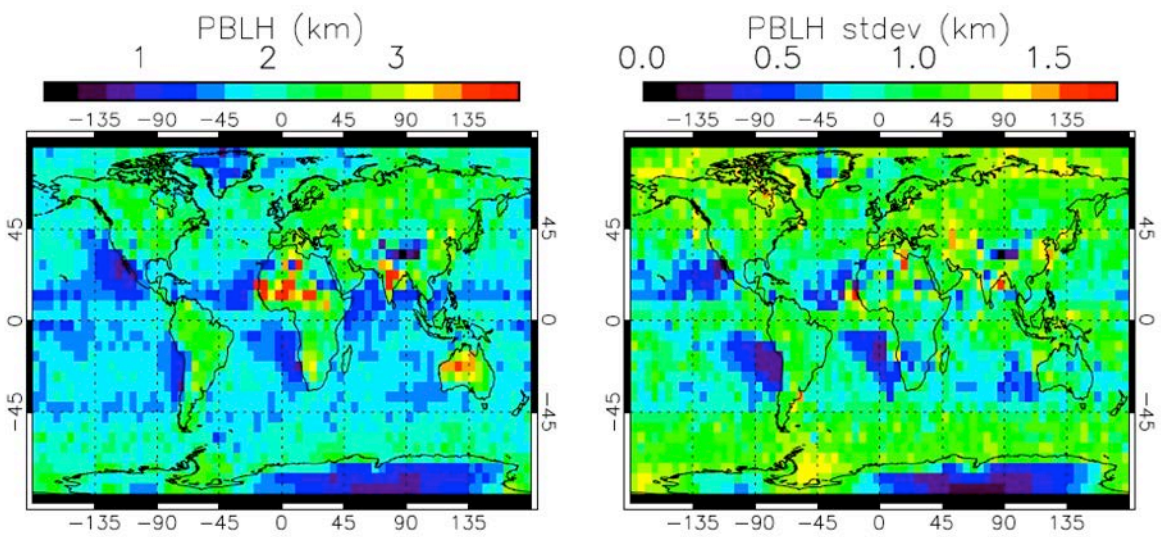

Figure 13. Median of seasonal PBLH climatology (left) and the median-absolute-deviation (MAD, right) from CALIPSO lidar measurement during MAM of 2013.

All ROPP PBLH diagnostics are directly compared with CALIPSO observation with the difference shown in Fig. 14. Overall, the tropical and subtropical oceans shows the minimum difference, except near the ITCZ. Whereas, ROPP is generally lower than CALIPSO over mid and high latitudes (e.g., north of 50°N and south of 50°S). Note, however, a systematic positive bias in ROPP PBLH over the Antarctic and the Greenland is shown, which is consistent with the difference from TAMU-CC PBLH in Fig. 11.

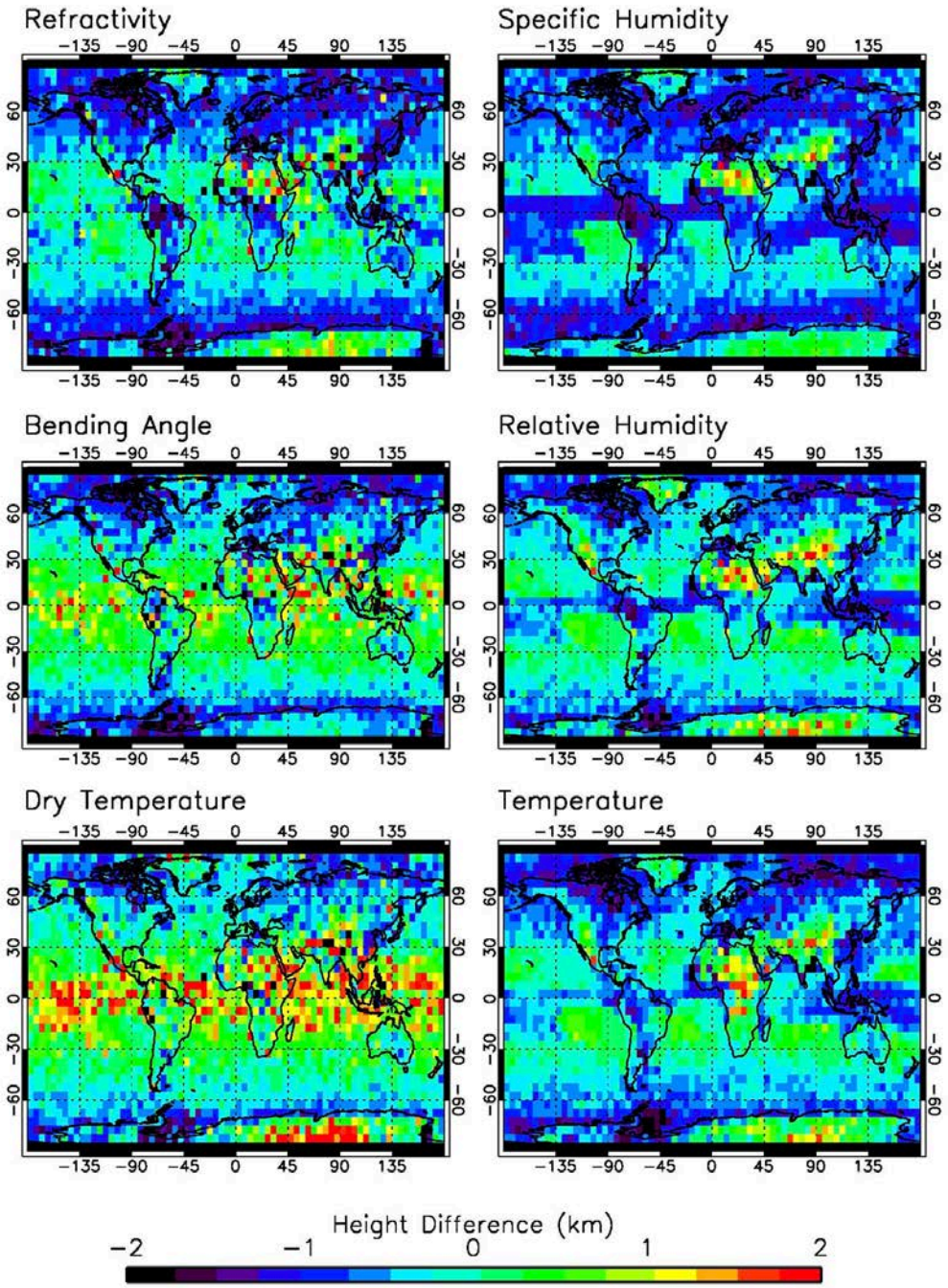

Figure 14. Difference of seasonal median ROPP PBLH climatology from CALIPSO during MAM of 2013.

4. Conclusions

In this report, the PBLH diagnostics based on three RO parameters (refractivity, bending angle and dry temperature) and three model parameters (specific humidity, relative humidity and temperature) during March-April-May of 2013 are generated from the ROPP PBLH diagnostic tool in the beta release of ROPP-9.0. Overall, the ROPP application tool is robust and easy to use, and the documentation is clear and very well-structured.

The seasonal climatology of six ROPP PBLHs is analyzed. The ROPP RO parameter based PBLH diagnostics are directly compared to the model parameter based PBLH. The ROPP PBLH diagnostics are also compared to the PBLH product generated by Xie at TAMU-CC that uses an independent but similar PBLH detection algorithm. Overall, the two PBLH products are very consistent except some positive bias in ROPP PBLH over the polar region, specially over the Antarctic and the Greenland. The difference over the polar region seems to be related to the special treatment of the PBLH detection algorithm in ROPP package in the presence of a shallow surface inversion (ROM-SAF Report 24, ROM SAF, 2016c). Clarification of such special treatment is needed.

The ROPP PBLH diagnostics are also compared to the CALIPSO PBLH that are derived based on the height of low level cloud or aerosol layers during the same three-month period. Overall, very similar pattern of global PBLH climatology is shown comparing the CALIPSO and the ROPP PBLH diagnostics, except the polar regions. Similar positive bias in ROPP PBLH over the Antarctic and the Greenland as seen in the comparison with the TAMU-CC data.

Some recommendations are summarized below for the PBLH diagnostic tool package:

1. Make the "minimum penetration height (h_{penet})" as an input parameter, which will allow more RO sounding profiles to be used for the elevated PBL study.
2. Introduce a new parameter called "$h_{\min}$" along with the "$h_{\max}$" to specify the valid vertical range in searching for the height of minimum (or maximum) gradient as the PBLH.
3. Make the vertical sampling of RO profiles to be 100 m or even smaller, e.g., 10-50 m to minimize the interpolation errors in the gradient method. This could be especially important for bending angle profile.
4. Add the "sharpness parameter" for each profile used for PBLH calculation.
5. Clarify the PBLH detection algorithm in the presence of surface inversion that are often observed over polar regions. The current ROPP PBLH algorithm is not consistent with the normal gradient method that simply detect the height of the minimum (or maximum) gradient as the PBLH, within the vertical range of 300 m to 5 km. It could lead to complication of interpreting the PBLH diagnostics.
    - Might be worthy of developing PBLH algorithm to detect the temperature inversion top height as the PBLH in the presence of surface inversion. It could be useful for model temperature and humidity profiles, which however, could be challenge to apply on RO sounding profiles due to the limited vertical resolution and the restricted deep penetration capability.

5. Acknowledgments

I would like to thank Drs. Ian Culverwell and Kent B. Lauritsen (DMI) for offer such a great opportunity to perform this visiting scientist activity. Especially I am grateful to Ian for providing the ROPP test dataset and offer useful discussion. I would also like to extend my appreciation to Dr. Loknath Adhikari at Texas A&M University – Corpus Christi, who offers help with the data processing.

6. References

Adhikari, L., Z. Wang, and D. Liu: Microphysical Properties of Antarctic polar stratospheric clouds and their dependence on tropospheric cloud systems, *J. Geophys. Res*., **115**, D00H18, doi:10.1029/2009JD012125, 2010.

Ao, C. O., Hajj, G. A., Meehan, T. K., Dong, D., Iijima, B. A., Mannucci, A. J., and Kursinski, E. R.: Rising and setting GPS occultations by use of open-loop tracking, *J. Geophys. Res*., **114**, D04101, doi:10.1029/2008JD010483, 2009.

Ao, C. O., D. E. Waliser, S. K. Chan, J.-L. Li, B. Tian, F. Xie, and A. J. Mannucci: Planetary boundary layer depths from GPS radio occultation profiles, *J. Geophys. Res.*, **117**, D16117, doi:10.1029/2012JD017598, 2012.

Beyerle, G., Schmidt, T., Wickert, J., Heise, S., Rothacher, M., Ko¨nig-Langlo, G., and Lauritsen, K. B.: Observations and simulations of receiver-induced refractivity biases in GPS radio occultation, *J. Geophys. Res*., **111**, D12101, doi:10.1029/2005JD006673, 2006.

Bony, S., and Dufresne J.-L.: Marine boundary layer clouds at the heart of tropical cloud feedback uncertainties in climate models, *Geophys. Res. Lett*., **32**, L20806, doi:10.1029/2005GL023851, 2005.

Bretherton, C. S., et al.: The EPIC 2001 stratocumulus study, *Bull. Am. Meteorol. Soc*., **85**, 967–977, doi:10.1175/BAMS-85-7-967, 2004.

Clement, A. C., Burgman R., and Norris J. R.: Observational and model evidence for positive low-level cloud feedback. *Science*, **325**, 460-464, DOI: 10.1126/science.1171255, 2009.

Duynkerke, P.G. and J. Teixeira: Comparison of the ECMWF Reanalysis with FIRE I observations: diurnal variation of marine stratocumulus. *J. Climate*, **14**, 1466-1478, 2001.

Garratt, J. R.: The atmospheric boundary layer, *Cambridge University Press*, 316pp., 1992.

Guo, P., Y.-H. Kuo, S. Sokolovskiy, and D. Lenschow, Estimating atmospheric boundary layer depth using COSMIC radio occultation data, *J. Atmos. Sci.*, **68(8)**, 1703-1713, doi:10.1175/2011JAS3612.1, 2011.

Ho, Shu-peng, Liang Peng, Richard A. Anthes, Ying-Hwa Kuo, and Hsiao-Chun Lin: Marine Boundary Layer Heights and Their Longitudinal, Diurnal, and Interseasonal Variability in the Southeastern Pacific Using COSMIC, CALIOP, and Radiosonde Data. *J. Climate*, **28**, 2856–2872, doi: http://dx.doi.org/10.1175/JCLI-D-14-00238.1, 2015.

Jordan, N. S., R. M. Hoff, and J. T. Bacmeister: Validation of Goddard Earth Observing System-version 5 MERRA planetary boundary layer heights using CALIPSO, *J. Geophys. Res*., **115**, D24218, doi:10.1029/2009JD013777, 2010.

Lauritsen, K. B., Syndergaard, S., Gleisner, H., Gorbunov, M. E., Rubek, F., Sørensen, M. B., and Wilhelmsen, H.: Processing and validation of refractivity from GRAS radio occultation data, *Atmos. Meas. Tech*., **4**, 2065-2071, doi:10.5194/amt-4-2065-2011, 2011.

ROM SAF, The Radio Occultation Processing Package (ROPP) User Guide. Part III: Pre-processor module, SAF/ROM/METO/UG/ROPP/004, Version 9.0, available at http://www.romsaf.org, 2016a.

ROM SAF, The Radio Occultation Processing Package (ROPP) User Guide. Part IV: Applications module, SAF/ROM/METO/UG/ROPP/005, Version 9.0, available at http://www.romsaf.org, 2016b.

ROM SAF, The calculation of planetary boundary layer height heights in ROPP, SAF/ROM/METO/REP/RSR/024, available at http://www.romsaf.org, 2016c.

Soden B. J. and Held I. M.: An Assessment of Climate Feedbacks in Coupled Ocean–Atmosphere Models. *J. Climate*, **19**, 3354–3360, 2006.

Sokolovskiy, S. V.: Tracking tropospheric radio occultation signals from low Earth orbit. *Radio Sci*., **36**, 483–498, 2001.

Sokolovskiy, S., Kuo, Y.-H., Rocken, C., Schreiner, W. S., Hunt, D., and Anthes, R. A.: Monitoring the atmospheric boundary layer by GPS radio occultation signals recorded in the open-loop mode, *Geophys. Res. Lett*., **33**, L12813, doi:10.1029/2006GL025955, 2006.

Stephens, G. L.: Cloud Feedbacks in the Climate System: A Critical Review. *J. Climate*, **18**, 237–273. doi: http://dx.doi.org/10.1175/JCLI-3243.1, 2005.

Winker , D. M., B. H. Hunt, and M. J. McGill: Initial performance assessment of CALIOP. *Geophys. Res. Lett.*, **34,** L19803, doi:10.1029/2007GL030135, 2007.

Wang, Z., G. Stephens, T. Deshler, C. Trepte, T. Parish, D. Winker, D. Liu, and L. Adhikari: Association of Antarctic polar stratospheric cloud formation on tropospheric cloud systems, *Geophys. Res. Lett*. **35**, L13806, doi:10.1029/2008GL034209, 2008.

Wyant, M. C., M. Khairoutdinov, and C. S. Bretherton: Climate sensitivity and cloud response of a GCM with a superparameterization. *Geophys. Res. Lett*., **33**, L06714, doi: 10.1029/2005GL025464, 2006.

Xie, F., Wu, D. L., Ao, C. O., Mannucci, A. J., and Kursinski, E. R.: Advances and limitations of atmospheric boundary layer observations with GPS occultation over southeast Pacific Ocean, *Atmos. Chem. Phys*., **12**, 903-918, doi:10.5194/acp-12-903-2012, 2012.

Xie, F., Visiting Scientist Report 21: Investigation of methods for the determination of the PBL height from RO observations using ECMWF reanalysis data, SAF/ROM/DMI/REP/VS21/001, Version 1.0, available at http://www.romsaf.org, 2014.

7. List of Acronyms

COSMIC	Constellation Observing System for Meteorology, Ionosphere, and Climate
C/NOFS	Communications/Navigation Outage Forecasting System (US)
ECMWF	European Centre for Medium-range Weather Forecasts
EUMETSAT	EUropean organisation for the exploitation of METeorological SATellites
GRACE–A/B	Gravity Recovery and Climate Experiment (US/Germany)
GRAS	GNSS Receiver for Atmospheric Sounding (onboard Metop)
GNSS	Global Navigation Satellite System
GPS	Global Positioning System (USA)
MetOp	Meteorological Operational polar satellites (EUMETSAT)
NetCDF	Network Common Data Form
NWP	Numerical Weather Prediction
RO	Radio Occultation
ROPP	Radio Occultation Processing Package
ROM SAF	Radio Occultation Meteorology (ROM) Satellite Application Facility (SAF) (EUMETSAT)
TerraSAR–X	German Earth Observation Satellite, carrying a Radio Occultation Sounder